Efficient production of S8 in interstellar ices: the effects of cosmic-ray-driven radiation chemistry and nondiffusive bulk reactions

Shingledecker, C.N.; Lamberts, T.; Laas, J.C.; Vasyunin, A.; Herbst, E.; Kästner, J.; Caselli, P.

The Astrophysical Journal, 888:52 (15pp), 2020 January 1 https://doi.org/10.3847/1538-4357/ab5360

Efficient Production of S_8 in Interstellar Ices: The Effects of Cosmic-Ray-driven Radiation Chemistry and Nondiffusive Bulk Reactions

Christopher N. Shingledecker[1,2,3], Thanja Lamberts[4], Jacob C. Laas[1], Anton Vasyunin[5,7], Eric Herbst[3,6], Johannes Kästner[2], and Paola Caselli[1]
[1] Max-Planck-Institut für extraterrestrische Physik, D-85748 Garching, Germany; cns@mpe.mpg.de
[2] Institute for Theoretical Chemistry University of Stuttgart Pfaffenwaldring 55, D-70569, Germany
[3] Department of Chemistry University of Virginia Charlottesville, VA, USA
[4] Leiden Institute of Chemistry, Gorlaeus Laboratories, Leiden University P.O. Box 9502, 2300 RA Leiden, The Netherlands
[5] Ural Federal University, Ekaterinburg, Russia
[6] Department of Astronomy University of Virginia Charlottesville, VA, USA
Received 2019 September 20; revised 2019 October 29; accepted 2019 October 30; published 2020 January 7

Abstract

In this work, we reexamine sulfur chemistry occurring on and in the ice mantles of interstellar dust grains, and report the effects of two new modifications to standard astrochemical models: namely, (a) the incorporation of cosmic-ray-driven radiation chemistry and (b) the assumption of fast, nondiffusive reactions for key radicals in the bulk. Results from our models of dense molecular clouds show that these changes can have a profound influence on the abundances of sulfur-bearing species in ice mantles, including a reduction in the abundance of solid-phase H_2S and HS, and a significant increase in the abundances of OCS, SO_2, as well as pure allotropes of sulfur, especially S_8. These pure-sulfur species—though nearly impossible to observe directly—have long been speculated to be potential sulfur reservoirs and our results represent possibly the most accurate estimates yet of their abundances in the dense interstellar medium. Moreover, the results of these updated models are found to be in good agreement with available observational data. Finally, we examine the implications of our findings with regard to the as-yet-unknown sulfur reservoir thought to exist in dense interstellar environments.

Unified Astronomy Thesaurus concepts: Cosmic rays (329); Astrochemistry (75); Interstellar molecules (849); Dense interstellar clouds (371); Interstellar dust processes (838)

Supporting material: machine-readable table

1. Introduction

The recent detection of several new sulfur-bearing molecules in the interstellar medium (ISM; Agundez et al. 2018; Cernicharo et al. 2018), as well as in comet 67P/Churyumov–Gerasimenko (67P/C-G) by the *Rosetta* orbiter (Calmonte et al. 2016) has, in part, spurred renewed interest in the chemistry of this malodorous element (Gorai et al. 2017; Danilovich et al. 2018; Drozdovskaya et al. 2018; Dungee et al. 2018; Hudson & Gerakines 2018; Morgan et al. 2018; Zakharenko et al. 2019). A number of recent studies have been motivated by the long-standing mystery regarding sulfur abundances in dense regions: namely, that though the total observed abundance of S-containing species in diffuse environments is approximately the cosmic value, in dense cores, sulfur appears to be depleted by up to several orders of magnitude (Prasad & Huntress 1982; Jenkins 2009; Anderson et al. 2013). One possible explanation for this apparently "missing" sulfur is that a great deal of it is incorporated into some as-yet-unknown molecule trapped in dust-grain ice mantles.

Over the past few years, quite a few attempts have been made to shed light on what this species might be using astrochemical models (Vidal et al. 2017; Semenov et al. 2018; Vastel et al. 2018; Vidal & Wakelam 2018; Laas & Caselli 2019; Le Gal et al. 2019). For instance, based on results from their simulations of the cold core TMC-1, Vidal et al. (2017) suggested that sulfur might exist mostly as either solid HS or H_2S, or as neutral atomic sulfur in the gas, depending on the age of the source. However, despite such predictions—and the fact that H_2S was recently detected by the *Rosetta* orbiter—thus far OCS remains the only sulfur-bearing species definitively observed in interstellar ices (Palumbo et al. 1997), though tentative detections of SO_2 have also been reported by Boogert et al. (1997) and Zasowski et al. (2009). More recently, Laas & Caselli (2019)—using a new chemical network that included a particularly comprehensive set of sulfur-related reactions—concluded that S was bound-up in organo-sulfur molecules in dust-grain ice mantles. More generally, though, there are a number of critical weaknesses in how current astrochemical codes simulate ice chemistry related to, e.g., chemical desorption, microscopic ice structure, reactant orientation, cosmic-ray-driven processes, and the dominant mechanism of bulk reactions. Though all of these topics are worthy of further study, we will focus here on the final two.

Cosmic rays and other forms of ionizing radiation, related to the first major shortcoming we address in this work, are ubiquitous in extraterrestrial environments. Unlike photons, cosmic rays are not quickly attenuated in dense molecular clouds (Ivlev et al. 2018; Padovani et al. 2018; Silsbee et al. 2018), and in fact drive much of the chemistry of these regions. Two major examples include the formation of H_3^+ following the ionization of molecular hydrogen (Herbst & Klemperer 1973), and the production of internal UV photons due to electronic excitation of H_2 (Prasad & Tarafdar 1983). Yet, as noted, interactions between these energetic particles and dust-grain ice mantles have until now only been considered in a

[7] Visiting Leading Researcher, Engineering Research Institute "Ventspils International Radio Astronomy Centre" of Ventspils University of Applied Sciences, Inženieru 101, Ventspils LV-3601, Latvia.

very limited, approximate way, in spite of a large body of previous laboratory work, which has proven that the irradiation of interstellar ice-analogs by energetic particles can drive a rich chemistry at even very low temperatures. Including such processes is likely important for accurately modeling solid-phase sulfur chemistry in dust-grain ice mantles. For example, experiments by Ferrante et al. (2008) have shown that OCS readily forms in S-containing ices bombarded by 0.8 MeV protons. Connections between this ion-driven "radiation chemistry" and interstellar sulfur were further strengthened by the detection of S_2 in the coma of comet 67P/C-G by Calmonte et al. (2016). In that work, the authors concluded that this S_2 likely formed in the presolar nebula via the radiolysis of species such as H_2S. In an attempt to improve how astrochemical models treat nonthermal processes, particularly those driven by cosmic rays, we have recently developed methods for including such radiation chemistry in rate-equation-based codes (Shingledecker & Herbst 2018). Our preliminary findings are that the addition of these new mechanisms generally improves the agreement between models and observations (Shingledecker et al. 2018); however, given the novelty of our approach, no modeling studies have yet been done which focus on the effects of cosmic-ray-bombardment on the abundances of sulfur-bearing species in ice mantles.

Another major source of uncertainty in current simulations of grain chemistry concerns reactions within the bulk of dust-grain ice mantles, such as whether or to what degree bulf diffusion is important, and if so, what the underlying mechanism behind this diffusion might be. Commonly, models today typically assume, for example, swapping (Öberg et al. 2009; Fayolle et al. 2011) or diffusion via interstitial sites (Lamberts et al. 2013; Chang & Herbst 2014; Shingledecker et al. 2017), where the energetic barriers to bulk diffusion, E_b^{bulk}, are taken to be some fraction of the desorption energy, E_D, and are highly uncertain. In Shingledecker et al. (2019b), we attempted to reduce this ambiguity by simulating well-constrained experiments, rather than the ISM. In our preliminary studies reported there, we found that the assumption that radicals within ices react via thermal diffusion leads to generally poor agreement between calculated and empirical results, due to the much slower chemistry in the simulations than what is shown to occur in the lab. Conversely, good agreement with experimental data was achieved by assuming that radicals in the ice react predominantly with their nearest neighbors, i.e., nondiffusively. These results are in qualitative agreement with a recent study by Ghesquière et al. (2018), who concluded that true bulk diffusion does not occur; rather, as temperatures increase, bulk species can be "passively" transported due to structural changes such as pore collapse or crystallization, or can "actively" diffuse along internal surfaces or cracks.

This work, therefore, is an attempt to build upon these recent investigations, and to examine what effect (a) cosmic-ray-driven radiation chemistry, and (b) the fast, nondiffusive reaction of radicals in the bulk have on the abundances of S-bearing species in simulations of dense cores, and moreover, what impact such additions have on the major sulfur reservoirs predicted by our models. The rest of the paper is organized as follows: in Section 2 we provide details regarding the code, chemical network, and underlying theory; in Section 3 we present our main results; and finally, the main conclusions of this study are summarized in Section 4.

2. Model and Theory

2.1. Astrochemical Code and Chemical Network

In this work, we have utilized the rate-equation-based astrochemical model, MONACO (Vasyunin et al. 2017), which we have previously modified as described in Shingledecker et al. (2019b). Specifically, these modifications allow for (1) the inclusion of cosmic-ray-driven radiation processes, including the formation and barrierless nondiffusive reaction of short-lived *suprathermal* species using the method of Shingledecker & Herbst (2018) and Shingledecker et al. (2018), and (2) the nondiffusive reaction of *thermal* radicals in the bulk of the ice. These modifications have been tested and shown to yield excellent agreement with experiments involving irradiated O_2 and H_2O ices (Shingledecker et al. 2019b).

In brief, the basis of the method described in Shingledecker & Herbst (2018) irradiation with the assumption that, for any grain species, A, collision by an energetic particle can lead to one of the following outcomes:

$$aA \rightsquigarrow aA^+ + e^- \tag{P1}$$

$$aA \rightsquigarrow aA^+ + e^- \rightarrow aA^* \rightarrow bB^* + cC^* \tag{P2}$$

$$aA \rightsquigarrow aA^* \rightarrow bB + cC \tag{P3}$$

$$aA \rightsquigarrow aA^*, \tag{P4}$$

where B and C are products, and a, b, and c are the stoichiometric coefficients. One can then calculate rate coefficients, k, for processes (P1)–(P4) using

$$k_{P1} = G_{P1}\left(\frac{S_e}{100\ \text{eV}}\right)\left(\Phi_{ST}\left[\frac{\zeta}{10^{-17}}\right]\right) \tag{1}$$

$$k_{P2} = G_{P2}\left(\frac{S_e}{100\ \text{eV}}\right)\left(\Phi_{ST}\left[\frac{\zeta}{10^{-17}}\right]\right) \tag{2}$$

$$k_{P3} = G_{P3}\left(\frac{S_e}{100\ \text{eV}}\right)\left(\Phi_{ST}\left[\frac{\zeta}{10^{-17}}\right]\right) \tag{3}$$

$$k_{P4} = G_{P4}\left(\frac{S_e}{100\ \text{eV}}\right)\left(\Phi_{ST}\left[\frac{\zeta}{10^{-17}}\right]\right). \tag{4}$$

where here, Φ_{ST} is the integrated Spitzer–Tomasko cosmic-ray flux (8.6 particles $\text{cm}^{-2}\,\text{s}^{-1}$) (Spitzer & Tomasko 1968), ζ is the H_2 ionization rate, and S_e is the so-called electronic stopping cross section, for which we use a average value of $S_e = 1.287 \times 10^{-15}\,\text{cm}^{-2}$ eV (Shingledecker et al. 2018; Shingledecker & Herbst 2018). The suprathermal species produced via processes (P2) and (P4) are critical for accurately reproducing energetic particle-driven chemistry at low temperatures (Abplanalp et al. 2016). In our model, we assume that, once formed, they quickly ($\sim 10^{-14}$ s) either react barrierlessly with a neighboring species or are quenched by the ice (Roessler 1991; Shingledecker et al. 2018). These rapid reactions involving suprathermal species will be considered as part of the radiolysis rather than post-radiolysis kinetics in the remainder of the paper, and are to be differentiated from rapid thermal reactions involving radicals in the bulk of the ice mantle.

Following Vasyunin et al. (2017), we assume the surface comprises the top four monolayers, from which species can desorb thermally or via the nonthermal processes of photodesorption or chemical desorption—with the latter calculated

Table 1
Reactions Updated Based on Results from ab Initio Calculations by Lamberts & Kästner (2017; LK17) and Lamberts (2018; L18)

Reaction	α (s^{-1})	β	γ (K)	T_0 (K)	Source
$H + H_2S \longrightarrow H_2 + HS$	2.2×10^{11}	0.48	1400	180	LK17
$H + CS \longrightarrow HCS$	3.3×10^{11}	0.50	100	35	L18
$H + H_2CS \longrightarrow H_2 + HCS$	3.6×10^{9}	0.95	1295	145	L18
$H + H_2CS \longrightarrow CH_3S$	1.6×10^{11}	0.50	290	85	L18
$H + H_2CS \longrightarrow CH_2SH$	6.4×10^{11}	0.50	30	65	L18
$H + CH_3SH \longrightarrow H_2 + CH_2SH$	1.2×10^{9}	1.20	1710	155	L18
$H + CH_3SH \longrightarrow H - 2 + CH_3S$	4.5×10^{10}	0.50	380	85	L18
$H + CH_3SH \longrightarrow H_2S + CH_3$	2.9×10^{10}	0.40	1060	70	L18

using the formalism described in Garrod et al. (2007) and occurring with the standard desorption efficiency of 1%. Oba et al. (2018) found the chemical desorption of the reaction system $H + H_2S \longrightarrow H_2 + HS$ and $H + HS \longrightarrow H_2S$ to have absolute lower and upper limits of 0.5% and 60%, respectively. The 1% efficiency we employ here for the reaction $H + HS \longrightarrow H_2S$ in particular is thus on the lower end of the spectrum; however, a detailed investigation of chemical desorption in this context falls beyond the scope of this paper. The third phase of our model, the bulk, consists of all monolayers below the top four (the surface). In addition to the previously mentioned radiolysis processes we have added, described above, it is assumed in the base MONACO code that photodissociation and reactions between bulk species can occur (Vasyunin et al. 2017).

Regarding tunneling through diffusion barriers, Senevirathne et al. (2017) and Asgeirsson et al. (2018) showed theoretically and Kuwahata et al. (2015) showed experimentally that, for atomic H, this effect is only important either for crystalline water surfaces or at very low temperatures (<10 K). However, results from Asgeirsson et al. (2018) suggest that there is a large spread in the rate coefficients, determined by the large range of binding energies on ASW surfaces, and thus, the most diffusive H atoms will be those bound lightly. To take the large spread in binding energies and resulting diffusive rate constants into account, for instance via a bimodal energy distribution (Cuppen & Garrod 2011), falls beyond the scope of the current paper. Therefore, based on the rate coefficients calculated in both theoretical studies, we use a modified first-order rate coefficient for H hopping on the high end of the spectrum, i.e., $\sim 4 \times 10^{9}\ s^{-1}$ at 10 K. For tunneling through chemical activation barriers, we use the standard formalism of Hasegawa et al. (1992) for H and H_2.

Our chemical network is based on the one recently developed by Laas & Caselli (2019). To this we have added a number of reactions, described below (see Appendix A). The most substantial additions to the network consisted of cosmic-ray-driven processes, including the radiolytic destruction of grain species, and reactions involving the resulting products. For the radiolysis processes, we have added both those given in Shingledecker et al. (2018, 2019b), as well as new radiolytic destruction routes for sulfur-bearing species—including pure-sulfur species from S_2 to S_8—with rate coefficients estimated using the method of Shingledecker & Herbst (2018). We have also included a number of solid-phase reactions identified in previous experimental studies of irradiated sulfur-bearing ices (Moore et al. 2007; Ferrante et al. 2008; Jiménez-Escobar & Muñoz Caro 2011; Chen et al. 2015).

2.1.1. Revised Competition Formula for Surface Reactions

Given the low temperatures of many interstellar environments, quantum mechanical tunneling through reaction activation energies (barriers) is a particularly attractive mechanism when considering the abundances of interstellar molecules. Thus, we have also included and/or updated a number of surface reactions involving sulfur-bearing species, given in Table 1, which occur via tunneling at low temperatures. In so doing, we have also updated how MONACO handles tunneling and competition more generally, using the updated theory presented below.

Currently, following Hasegawa et al. (1992), it is common to multiply R_{AB}, the rate of diffusive surface reactions between some two species, A and B, by a factor, κ_{AB}, which characterizes the probability of reaction. For exothermic barrierless reactions $\kappa_{AB} = 1$, while for exothermic reactions with some activation energy, E_a, $\kappa_{AB} \in [0, 1]$. The probability of overcoming E_a (in units of K) per pass thermally is simply

$$\kappa_{\rm therm}^{\rm AB} = \exp\left(-\frac{E_{\rm a}}{T}\right), \tag{5}$$

where T is the temperature. However, if there is at least one light reactant, e.g., H or H_2, or a process involving the transfer of H from one molecule to another, there is a chance that the reaction could proceed more efficiently at low temperatures via tunneling. Following Tielens & Hagen (1982), one can approximate this probability by assuming a rectangular barrier of height E_a and width a:

$$\kappa_{\rm tunn}^{\rm AB} = \exp\left[-2\left(\frac{a}{\hbar}\right)\sqrt{2\mu E_a}\right]. \tag{6}$$

Here, μ is a reduced or effective mass of the reactants and a is commonly assumed to be 1 Å. A more realistic value of κ_{AB} for tunneling was derived by Herbst & Millar (2008), which treats the competition between tunneling and diffusion, i.e.,

$$\kappa_{\rm HM}^{\rm AB} = \frac{k_{\rm tunn}}{k_{\rm tunn} + k_{\rm hop,A} + k_{\rm hop,B}}, \tag{7}$$

where $k_{\rm hop,A}$ and $k_{\rm hop,B}$ are the hopping rates for A and B, respectively (Herbst & Millar 2008), given by

$$k_{\rm hop,A} = \nu_0^{\rm A} \exp\left(-\frac{E_{\rm b}^{\rm A}}{T}\right) \tag{8}$$

and the first-order tunneling rate coefficient is given by

$$k_{\rm tunn} = (\nu_0^{\rm A} + \nu_0^{\rm B}) \times \kappa_{\rm tunn}^{\rm AB}, \tag{9}$$

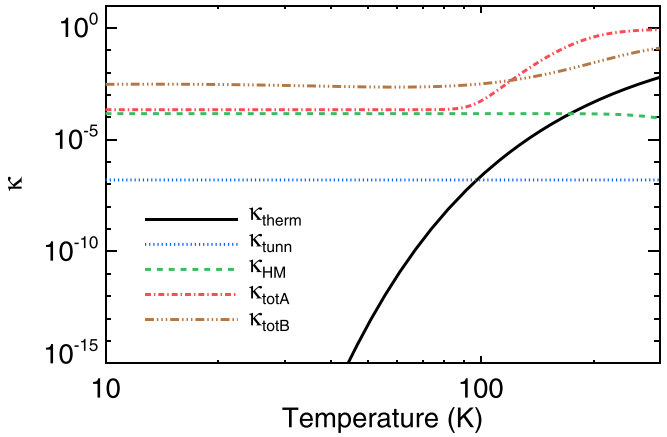

Figure 1. Values of κ calculated using a number of methods (see the text) for the surface reaction $H + H_2S \rightarrow H_2 + HS$. Here, the dotted–dashed line (κ_{totA}) uses $k_{react} = k_{tunn} + k_{therm}$, whereas the triple dotted–dashed line (κ_{totB}) uses $k_{react} = k_{inst}$. Parameters for instanton results were taken from Lamberts & Kästner (2017).

with ν_0 in the above expressions being the well-known attempt frequency (Landau & Lifshitz 1976), which typically has a value on the order of $10^{12}\,s^{-1}$ (Herbst & Millar 2008) for physisorption.

In astrochemical models, a common practice is to compare κ^{AB}_{therm} with either κ^{AB}_{tunn} or κ^{AB}_{HM} at every temperature, and to select the largest of these (Taquet et al. 2012; Garrod 2013; Vasyunin & Herbst 2013). Shown in Figure 1 are these values over 10–150 K for the surface reaction

$$H + H_2S \rightarrow H_2 + HS \tag{10}$$

where, for illustration, we have utilized an activation energy of 1530 K (Lamberts & Kästner 2017) and assumed both reactants encounter one another via thermal diffusion.

Because astrochemical networks typically do not include separate reactions for the formation of products via the thermal or tunneling mechanism, however, the ultimate question of interest in models is not the mechanism by which a given reaction proceeds, but rather, whether it proceeds at all at a given temperature, and if so, with what rate. Thus, we here propose a new formalism for determining the probability of reaction, given simply by

$$\kappa^{AB}_{tot} = \frac{k_{react}}{k_{react} + k_{hop,A} + k_{hop,B}} \tag{11}$$

$$k_{react} = k_{tunn} + k_{therm}. \tag{12}$$

Thus, κ^{AB}_{tot} gives the total probability that a given reaction with a barrier will proceed—either thermally or via tunneling—when there is a competing chance that the reactants can diffuse away from each other. One advantage of Equation (11) is that it eliminates the need to explicitly compare the thermal versus nonthermal probabilities at every temperature in the model, thereby reducing computational expense. Moreover, in simulations of hot core or shocks, use of Equation (11) will reduce potential discontinuities that can detrimentally affect numerical convergence. Because desorption is typically treated as a separate, distinct process in many astrochemical models, we do not include a desorption rate in the denominator of Equation (11) to prevent double counting of the phenomenon. We should note that one disadvantage of Equation (6) is that, if $k_{tunn} = k_{therm}$, k_{react} will be a factor of 2 too large; however, the effects on the total result will likely be negligible.

For the tunneling factor in Equation (11), one can use either the standard square potential, given in Equation (6), or alternatively, one can employ more realistic values, such as those obtained via instanton theory (Rommel et al. 2011; Kästner 2014), which has recently been used to fruitfully study a number of reactions of astrochemical interest (Shingledecker et al. 2019a). In one such study by Lamberts & Kästner (2017), the role of tunneling in reaction (10) was investigated. For the reaction

$$A + B \rightarrow [A \cdots B] \rightarrow C + D, \tag{13}$$

the first-order decay rates for the pre-reaction complex (PRC), $[A\cdots B]$, as described in Lamberts et al. (2016), can be fit to a modified Arrhenius equation originally proposed by Zheng & Truhlar (2010)

$$k_{inst} = \alpha\left(\frac{T}{300\ K}\right)^{\beta} \exp\left(-\gamma\frac{T + T_0}{T^2 + T_0^2}\right) s^{-1} \tag{14}$$

which can account for the approximately constant value of the rate coefficient at low temperatures due to tunneling. The resulting rate for the formation of products C and D from the PRC can be expressed as

$$\frac{d[A \cdots B]}{dt} = -k_{inst}[A \cdots B]. \tag{15}$$

When available, one can use the results of such detailed calculations in Equation (11), as shown in Figure 1 for reaction (10).

Here, it is important to stress two points regarding the kinds of reactions that proceed via the diffusive Langmuir–Hinshelwood mechanism, and for which the use of a competition formula is appropriate, namely that (1) the value of κ cannot exceed unity and (2) that regardless of the efficiency of overcoming the reaction barrier, the reactants still must encounter one another on the grain surface. Consequently, in the limit of highly efficient thermal activation over or tunneling through the reaction barrier, the rate of an exothermic reaction with a barrier approaches that of a barrierless exothermic reaction.

Finally, for thermal bulk reactions which can proceed via tunneling, we have employed a different expression than Equation (11), as it is assumed in that formula that the reactants have encountered one another diffusively, and there exists a nonzero chance that they can, given the presence of a finite chemical activation barrier, diffuse away from each other. For the bulk, we do not wish to assume that such diffusion occurs. Thus, we employ the following expression for κ^{AB} in cases where there is evidence of tunneling:

$$\kappa^{AB}_{bulk} = \frac{k_{react}}{\nu^A_0 + \nu^B_0}. \tag{16}$$

Here, as with Equation (12), the numerator can be either the sum of a low-temperature and high-temperature term, or as in Equation (14), a single temperature-dependent expression that accounts for both. In Equation (16), k_{react} characterizes the rate at which the PRC decays, and the denominator, the sums of the characteristic frequencies, approximates the number of times per second this complex can do so—with the quotient of the two thus accounting for the average probability that any such attempt will result in a successful reaction.

Table 2
Physical Conditions

Parameter	Value
n_{gas}	10^4 cm^{-3}
A_V	10 mag
ζ	1.3×10^{-17} s^{-1}
T_{gas}	10 K
T_{dust}	10 K

Table 3
Initial Elemental Abundances

Element	Relative Abundance	Source
H	0.9999	
H_2	5.0000×10^{-5}	
He	9.5500×10^{-2}	Przybilla et al. (2008)
O	5.7544×10^{-4}	Przybilla et al. (2008)
C^+	2.0893×10^{-4}	Przybilla et al. (2008)
N	5.7544×10^{-5}	Przybilla et al. (2008)
Mg^+	3.6308×10^{-5}	Przybilla et al. (2008)
Si^+	3.1623×10^{-5}	Przybilla et al. (2008)
Fe^+	2.7542×10^{-5}	Przybilla et al. (2008)
S^+	1.6600×10^{-5}	Esteban et al. (2004)
Na^+	1.7400×10^{-6}	Asplund et al. (2009)
Cl^+	2.8800×10^{-7}	Esteban et al. (2004)
P^+	2.5700×10^{-7}	Asplund et al. (2009)
F	3.6300×10^{-8}	Asplund et al. (2009)

2.2. Physical Conditions and Model Details

To investigate the role of radiation chemistry and nondiffusive bulk reactions on the abundances of sulfur species in dense interstellar regions, we have run simulations of generic cold cores using physical conditions and initial elemental abundances taken from Laas & Caselli (2019), and listed in Tables 2 and 3.

We have carried out five sets of simulations, as listed in Table 4. Of these five, the results of two (A and B) are discussed here in detail and the results of the three others (C, D, and E) are in Appendix B. Our "fiducial" model, here referred to as Model A, uses standard treatments for surface and bulk chemistry as described in Vasyunin et al. (2017). Conversely, in Model B, we enable (i) cosmic-ray-driven radiation chemistry as described in Shingledecker et al. (2018), including both the radiolytic destruction of grain mantle species and the subsequent production of electronically excited suprathermal species and thermal fragments, including radicals; (ii) a nondiffusive bulk-reaction mechanism for a number of key bulk radicals relevant to our investigation; and finally (iii) the modified competition formula proposed here. Given the novelty of (ii) in the context of astrochemical modeling, we here take an incremental approach to its implementation in our code as an initial test of its effect on the overall chemistry and composition of dust-grain ice mantles. In particular, we restrict the number of species that react via this nondiffusive mechanism to either those previously shown to be well modeled in this way (Shingledecker et al. 2019b), or most directly relevant for the grain chemistry of sulfur-bearing species, specifically, O, OH, HO_2, HO_3, H, HS, NS, HSO, C, S, and CS.

3. Results and Discussion

The results of our simulations for models A and B are presented in Figures 2–4. In Figures 2 and 3, the gas (blue), surface (green), and bulk (red) abundances with respect to molecular hydrogen of a number of sulfur-bearing species are shown. Where available, gas-phase abundances from dense cloud observations are represented by blue hatched bars, with values taken from Table 4 of Laas & Caselli (2019). In all figures, results from Model A are depicted with dashed lines, and those from Model B by solid lines. We note that unless otherwise stated, reactions referred to here describe processes occurring within the bulk of the ice.

Table 5 compares the abundances of a number of sulfur-bearing species in the comet nucleus (inferred from analysis of gas-phase coma material measured by *Rosetta*), with the total ice abundance (surface+bulk) in Models A and B. Calculated abundances listed in Table 5 are those at model times of $\sim 2 \times 10^6$ yr (corresponding to an ice ca. 100 monolayers thick) because, as we show below, this is the point in our simulations of best agreement with existing observational data. Our results at this time, therefore, may provide an interesting point of comparison between ISM values and those from much older solar system objects. In addition to the obvious differences in age; however, we stress that care should also be taken in interpreting the data in Table 5, since the cometary abundance of some species, e.g., S_2 and SO, may have been enhanced due to the fragmentation of some larger parent species either within the mass spectrometer on board *Rosetta*, or directly within the nucleus of 67P/C-G.

Of the species whose abundances are depicted in Figures 2 and 3, eight have been detected in cold dense clouds, namely H_2S, C_2S, H_2CS, CS, SO, SO_2, NS, and OCS (see Laas & Caselli 2019 and references therein). These two figures show that our models agreeably reproduce the abundances of most of these observed species at around $(1–2) \times 10^6$ yr—a reasonable time for such dense clouds—with the exception of CS and, to a lesser degree, H_2S, both of which are overproduced in the gas. One can see, moreover, that while the novel processes included in Model B have profound effects on the bulk abundances of most species shown, as expected, the two models predict generally similar gas and surface abundances.

3.1. Effect of Novel Bulk Processes

3.1.1. Radicals

Not surprisingly, based on our previous results described in Shingledecker et al. (2019b), one clear effect of our nondiffusive mechanism is a significant reduction in the abundances of radicals in the bulk, as can be seen by, e.g., NS, CS, and S in Figure 3. Models often predict large abundances of these reactive species in interstellar ices. It may be, though, that such results represent worrying departures from physical realism, a supposition supported somewhat surprisingly by the results of Greenberg & Yencha (1973) in their well-known work describing the dramatic phenomenon they called "grain explosions." There, Greenberg and Yencha speculated that such explosions were driven by the exothermic reactions of radicals trapped in the ice. Critically, though, they note that in reality, the collective concentration of these reactive species should not exceed ~1% due to the rapidity with which they react both with themselves and their neighbors. This implies that S, HS, and other reactive species

Table 4
Processes Enabled in the Simulations Carried out for this Work

Process	Model A	Model B	Model C	Model D	Model E
Cosmic-ray-driven chemistry	no	yes	no	yes	no
Nondiffusive bulk reactions	no	yes	yes	no	no
Modified competition formula	no	yes	yes	yes	yes

can most likely be ruled out as significant reservoirs of sulfur in dust-grain ice mantles.

3.1.2. H_2S

Hydrogen sulfide, H_2S, is a species often predicted to be a major reservoir of sulfur in dense regions (Esplugues et al. 2014; Holdship et al. 2016; Danilovich et al. 2017; Vidal et al. 2017), because it forms readily from sulfur atoms adsorbed onto grain surfaces via

$$\mathrm{H} + \mathrm{S} \longrightarrow \mathrm{HS} \tag{17}$$

followed by

$$\mathrm{H} + \mathrm{HS} \longrightarrow \mathrm{H_2S}. \tag{18}$$

Thus, as dust-grain ice mantles grow, H_2S is trapped in the bulk where, being resistant to further reaction to hydrogen due to the large reaction barrier, it remains by far the most abundant sulfur-bearing species on the grain.

However, there are two main problems with the hypothesis that hydrogen sulfide is the primary sulfur reservoir in dust-grain ice mantles. First, in addition to driving the formation of H_2S, atomic hydrogen can also efficiently destroy hydrogen sulfide even at low temperatures via tunneling, as was shown recently by Lamberts & Kästner (2017). The second, major flaw is that it is apparently not sufficiently abundant in dust-grain ice mantles to be detected (Smith 1991; Boogert et al. 2015).

As shown in Figure 2, in agreement with past modeling results, Model A likewise predicts that a substantial fraction of the total sulfur is locked in H_2S at late times. Strikingly, though, in Model B, bulk abundances of H_2S are reduced by ∼5–6 orders of magnitude compared with those in Models A. This reduction in bulk abundance is mainly due to two factors at play in Model B; namely, (1) the increased destruction of H_2S in the bulk by cosmic rays, as well as reactions with atoms and radicals, especially OH, and, (2) the fact that in Model B, bulk reactions are not dominated solely by those involving light, mobile species such as atomic hydrogen, and thus, that the HS produced in reaction (10) does not quickly reform H_2S via (18).

The contrasting results predicted by Models A and B serve as a good illustration of the kinds of chemistry that characterize reactions in the bulk, depending on the assumptions made regarding the underlying mechanisms. Specifically, in the traditional diffusive approach, bulk chemistry is dominated by reactions involving atomic hydrogen, given its abundance, reactivity, and high mobility, whereas our new nondiffusive approach allows other radicals, such as HS—which would otherwise either build up or form H_2S—to play a more active role.

From Table 5, one can see that both models are within an order of magnitude of the H_2S abundance measured by *Rosetta*, though with the Model A result somewhat closer to the cometary value. Further comparison between the average $[H_2S]/[H_2O]$ upper limit derived by Smith (1991) of 1.5% in dense interstellar clouds, and our calculated value at 2 Myr confirms that the Model A result of 3% is likely too large, with the Model B value of 0.4% being in better agreement with the observational data in this regard.

3.1.3. OCS

Carbonyl sulfide, OCS, the only sulfur-bearing species definitively detected in interstellar ices to date (Palumbo et al. 1997; Aikawa et al. 2012), serves as an important means by which we can quantitatively compare how accurately our models are simulating the real chemistry of dust-grain ice mantles. From Figure 3, one can see that the bulk abundance of OCS is substantially higher in Model B than Model A. This increase is driven mainly by the grain reaction

$$\mathrm{S} + \mathrm{CO} \longrightarrow \mathrm{OCS}, \tag{19}$$

which occurs with only a negligible rate in Model A due to the slow diffusion of the reactants at 10 K.

Moreover, when we compare our results with the available observational findings, it becomes clear that Model B provides a much better match with existing empirical data. Specifically, Model B reproduces the solid OCS relative abundance of $\sim 10^{-6}$, as well as the ice/gas abundance ratio of $\sim 10^{3}$ observed by Aikawa et al. (2012). Further comparison with [OCS]/[CO] abundance ratios measured by Palumbo et al. (1997), listed in Table 6, shows again that the results of Model B are in better agreement with previous observations. One draws a similar conclusion from a comparison with data from the *Rosetta* mission which, again, more closely match calculated OCS ice abundances from Model B.

3.1.4. SO_2

Although OCS remains the only definitively detected sulfur-bearing species in interstellar ices, there is also tentative evidence for the presence of sulfur dioxide, SO_2, based on observations by Zasowski et al. (2009) and Boogert et al. (1997), who report values of $[SO_2]/[H_2O] \approx 0.5\%$ and ≈0.1%–1%, respectively. That SO_2 is indeed an important component of interstellar ices is perhaps hinted at by the ubiquity of sulfur dioxide frost on the Jovian moon, Io—the surface of which is dominated by abundant sulfur-bearing molecules, particularly S_8 (Carlson et al. 2007). Thus, SO_2 represents another key species useful in determining the relative accuracy of our simulations.

In this regard, as shown in Figure 3, Model B again performs better: predicting a bulk abundance ∼5 orders of magnitude greater than Model A. As with OCS, this increase is due to eliminating the reliance on thermal diffusion within the ice mantle, thereby allowing sulfur dioxide to form efficiently in situ via

$$\mathrm{SO} + \mathrm{OH} \longrightarrow \mathrm{SO_2} + \mathrm{H}, \tag{20}$$

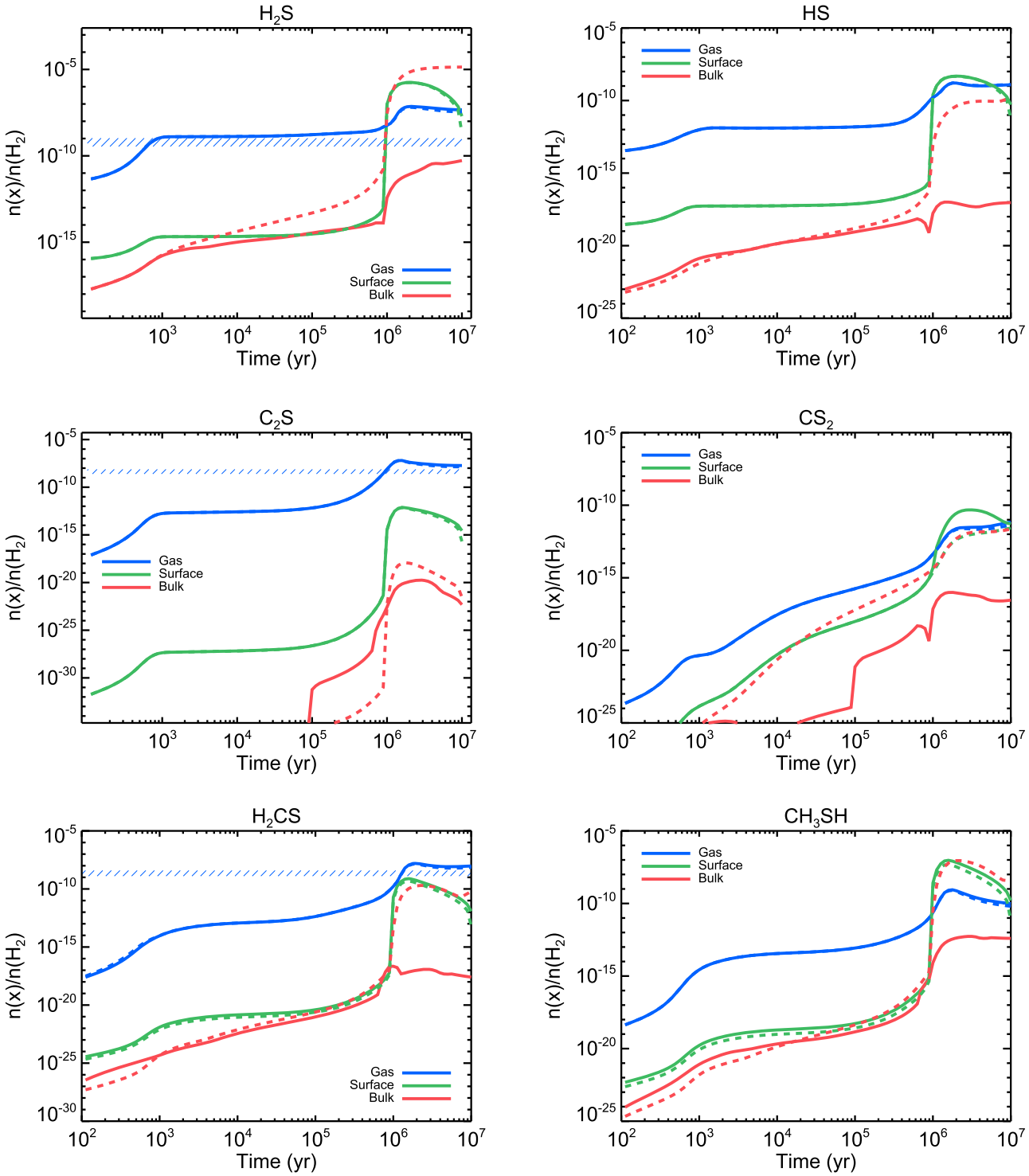

Figure 2. Calculated abundances of H_2S, HS, H_2CS, C_2S, CS_2, and CH_3SH in models A (dashed line) and B (solid line). Gas-phase observational abundances for dense clouds, where available, are represented by horizontal blue hatched bars (see Laas & Caselli 2019 and references therein.).

unlike in Model A, where SO_2 on grains is predominantly the result of accretion from the gas.

Comparing our calculated sulfur dioxide abundance with those from Zasowski et al. (2009) and Boogert et al. (1997), we note that Model B reproduces their reported $[SO_2]/[H_2O] \approx 0.5\%$ at ca. 2 Myr, with the abundance in Model A at that time being $\approx 10^{-6}\%$. Interestingly, *Rosetta* measured an SO_2 abundance of $[SO_2]/[H_2O] \approx 0.1\%$, remarkably similar to what has been reported in these tentative detections. The SO_2 ice abundance predicted by Model B is therefore in agreement with both cometary results as well as the existing ISM values, with Model A likewise underproducing SO_2 in both cases by $\sim$5 orders of magnitude.

3.1.5. Sulfur Allotropes

Over 30 different allotropes of sulfur are currently known—more than any other element (Steudel & Eckert 2003). Of these,

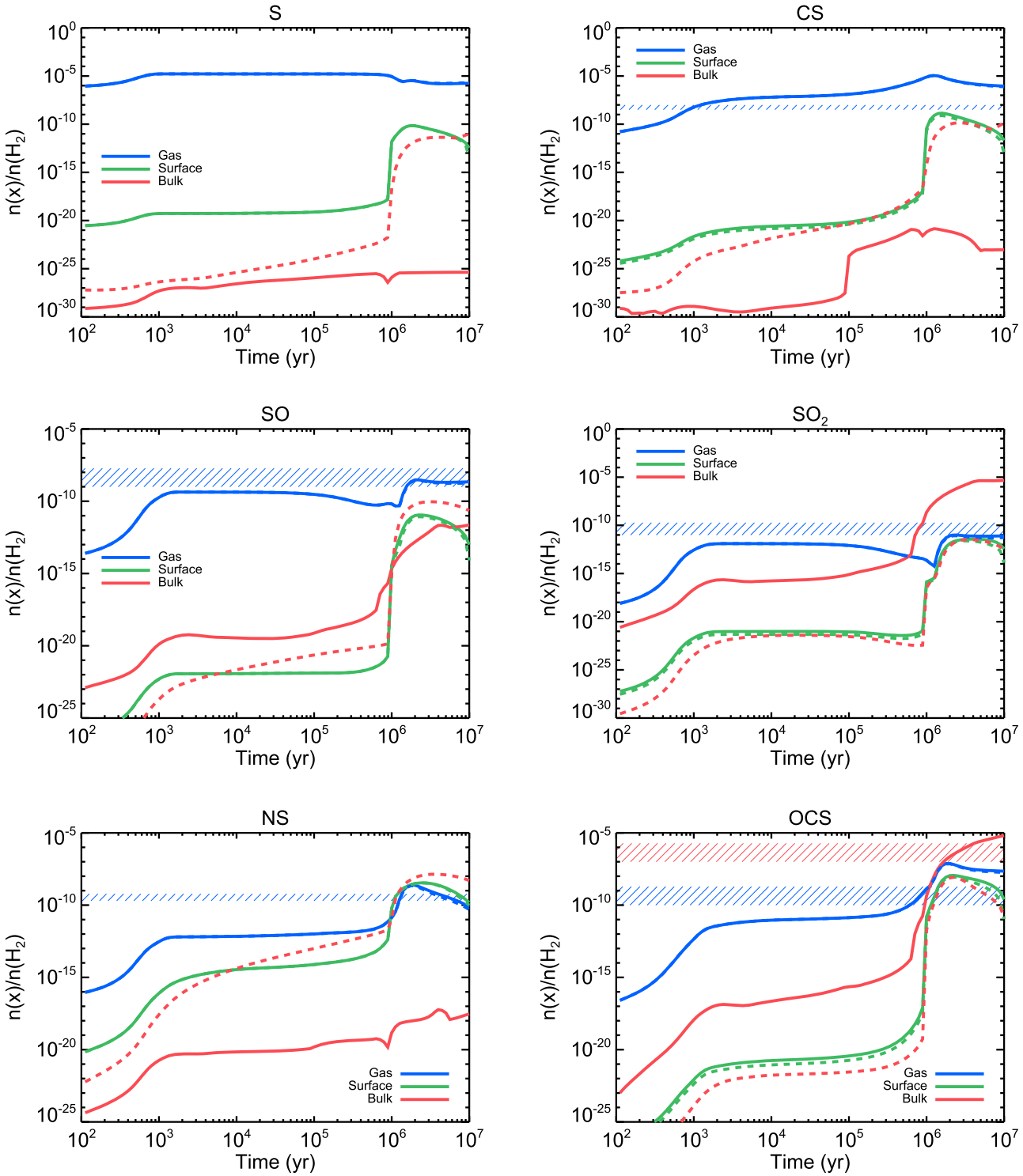

Figure 3. Calculated abundances of S, CS, SO, SO_2, NS, and OCS in models A (dashed line) and B (solid line). Gas-phase observational abundances for dense clouds, where available, are represented by horizontal blue hatched bars (see Laas & Caselli 2019 and references therein).

S_8—also called octasulfur or simply "elemental sulfur"—is the most stable, and by far the most abundant in nature. Octasulfur, one form of which has the bright-yellow color historically associated with deposits of the pure element on Earth (Steudel 1982), can also be seen on other solar system bodies, such as Io, which is thought to have a surface rich in S_8 based, in part, on its coloration and the observation of S_8 features in UV–Vis Solar reflectance spectra (Carlson et al. 2007).

One of the most interesting results of this study is the combined effect of radiation chemistry and nondiffusive bulk reactions on the abundances of S_n ($n \in [2, 8]$). As can be seen from Figure 4, the increased efficiency of bulk chemistry in Model B results in substantially higher abundances for the all sulfur allotropes in our network, in particular S_8.

The formation of these pure-sulfur species begins with S_2, which in Model B occurs mainly via (Mihelcic & Schindler 1970)

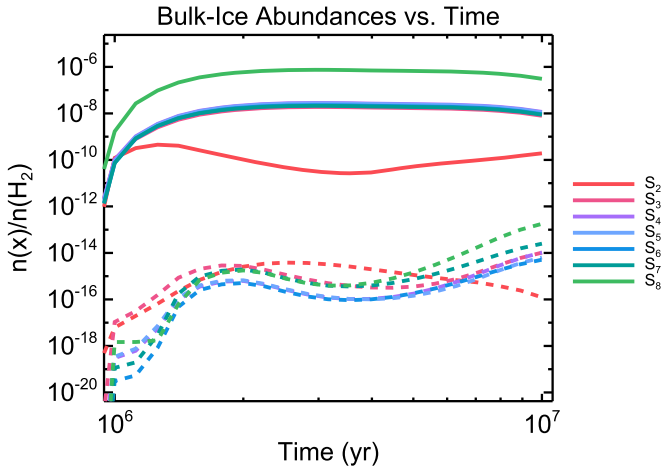

Figure 4. Abundances of sulfur allotropes (S_n, $n \in [2, 8]$) within the bulk in models A (dashed line) and B (solid line).

Table 5
Total Calculated Grain Abundances (Surface+bulk) of Sulfur-bearing Species Relative to H_2O at $t \approx 2 \times 10^6$ yr, as well as Derived ice Abundances for comet 67P/C-G Taken from Calmonte et al. (2016)

Molecule	Model A	Model B	67P/Churyumov–Gerasimenko
H_2S	3×10^{-2}	4×10^{-3}	$(1.10 \pm 0.05) \times 10^{-2}$
OCS	4×10^{-5}	5×10^{-4}	$(4.08 \pm 0.09) \times 10^{-4}$
SO	2×10^{-7}	3×10^{-8}	$(7.1 \pm 1.1) \times 10^{-4}$
SO_2	4×10^{-9}	7×10^{-4}	$(1.27 \pm 0.03) \times 10^{-3}$
CS_2	2×10^{-9}	7×10^{-8}	$(5.68 \pm 0.18) \times 10^{-5}$
S_2	6×10^{-12}	2×10^{-7}	$(1.97 \pm 0.35) \times 10^{-5}$
CH_3SH	3×10^{-4}	1×10^{-4}	$(2.85 \pm 1.11) \times 10^{-5}$[a]
H_2CS	1×10^{-6}	1×10^{-6}	$(2.67 \pm 0.75) \times 10^{-6}$[b]

Notes.
[a] 2014 October—Table 4 of Calmonte et al. (2016).
[b] 2015 March 28 12:14—Table 5 of Calmonte et al. (2016).

Table 6
Observed and Calculated [OCS]/[CO] Abundance Ratios in Interstellar Dust-grain Ice Mantles

Source	Abundance (%)
Observed	
W33A	5.0×10^{0}
AFGL 989	8.0×10^{-1}
Mon R2 IRS2	6.5×10^{-1}
AFGL 961E	$<1.0 \times 10^{0}$
AFGL 490	$<2.6 \times 10^{0}$
NGC 2024 IRS 2	$<8.0 \times 10^{-1}$
OMC 2 IRS 3	$<1.6 \times 10^{0}$
Elias 16	$<8.0 \times 10^{0}$
Calculated	
Model A	1×10^{-2}
Model B	7×10^{-1}

Note. Observational values are taken from Palumbo et al. (1997), and calculated values are those at $t \approx 2 \times 10^6$ yr.

$$S + HS \longrightarrow S_2 + H. \quad (21)$$

Once produced, disulfur can then dimerize to form S_4 which can, for example, either react with S to form S_5 or with S_2 to form S_6. Conversely, in Model A, S_2 in the mantle comes either from the accretion of gas-phase S_2 or, to a lesser degree, the surface reaction (Sendt et al. 2002)

$$H + S_2H \longrightarrow S_2 + H_2. \quad (22)$$

The results of Model B are in agreement with previous experimental studies on interstellar ice analogues, which show that S_8 can form readily at low temperatures in both UV- (Jiménez-Escobar & Muñoz Caro 2011; Chen et al. 2015) and proton- (Garozzo et al. 2010) irradiated ices; however, these are the first simulations—to the best of our knowledge—which show that the formation of sulfur allotropes can indeed be efficient in real astrophysical environments.

Intriguingly, the presence of elemental sulfur in cometary nuclei was suggested recently by the detection of S_2, S_3, and S_4 during the *Rosetta* mission, which Calmonte et al. (2016) noted were likely formed from a compound such as S_8. A comparison of our calculated abundances with *Rosetta* measurements of S_2 shows, again, that Model B yields values closer to the available data.

3.1.6. Sulfur Reservoir

Shown in Figure 5 are the dominant sulfur-bearing species as a function of time in Models A and B. At times before ca. 1 Myr, both models predict similar progressions of the dominant sulfur-bearing species from the initial S^+, to neutral atomic sulfur, and finally CS. After 1 Myr, Models A and B likewise show similar degrees of depletion of gas-phase sulfur onto grains, though differences in how bulk chemistry is treated in the two models lead to strikingly dissimilar predicted abundances for sulfur-bearing species in the ice.

Model A—our fiducial simulation—predicts an ice in which nearly all sulfur exists as H_2S. This high hydrogen sulfide abundance has been characteristic of previous model results (Holdship et al. 2016; Vidal et al. 2017), and is the natural outcome of a diffusive surface and bulk chemistry dominated by reactions with atomic hydrogen, given its reactivity, mobility, and abundance (Jiménez-Escobar & Muñoz Caro 2011). One exception was the recent study by Laas & Caselli (2019), who found SO and OCS to be more abundant than H_2S on the grain. Though our network is based on the one presented in that work, their use of a two-phase model means that diffusion and desorption are more efficient than in three-phase codes such as the one we use in this study—resulting in a greater similarity between the results of Laas & Caselli (2019) and those of Model B.

One alternative candidate for the long-sought sulfur reservoir is suggested by our Model B results. In Figure 5, one can see three major classes of sulfur-bearing species on grains at late times, namely, OCS, SO_2, and the allotropes. It has been speculated previously by Palumbo et al. (1997) and Garozzo et al. (2010) that the presence of large amounts of S_8 (and related species) could resolve the missing-sulfur problem. Unfortunately, S_8 has no strong IR-active modes and it is therefore very difficult to observationally constrain its abundance in real dust-grain ice mantles (Palumbo et al. 1997). Even observations of post-shocked material, as done recently by Holdship et al. (2019), also might not clearly reveal the presence of abundant sulfur allotropes, because of their

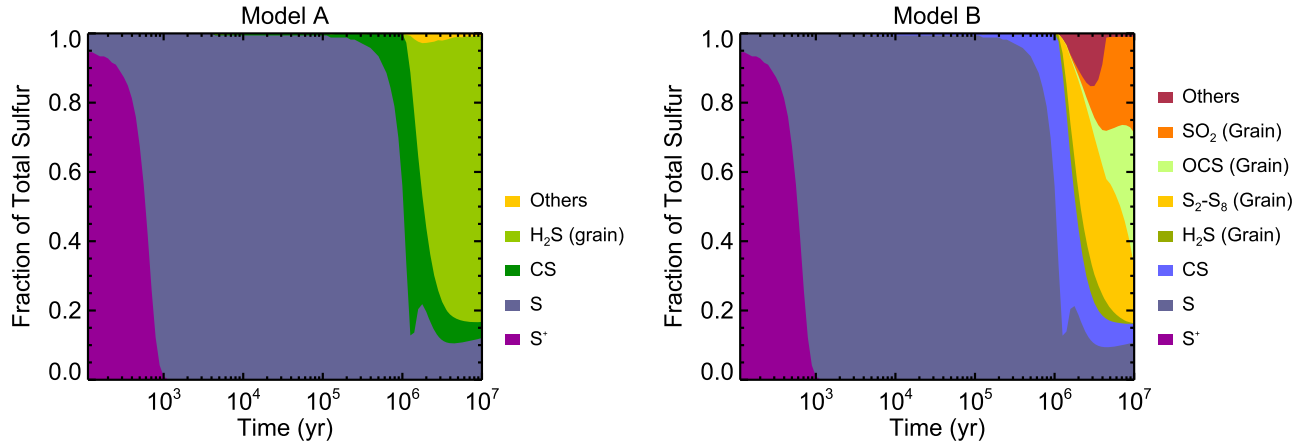

Figure 5. Main sulfur-bearing species in Model A (left) and Model B (right).

refractory nature or the difficulty of observing even their dissociation products, e.g., S_4. Nevertheless, it was recently inferred by Kama et al. (2019), that much of the sulfur in protoplanetary disks is locked away in such a refractory compound with physical characteristics consistent with those of S8.

Shown in Figure 8 of Appendix B are the corresponding plots showing the major sulfur-bearing species predicted by Models C–E. Figure S4 shows that, of the processes listed in Table 4, nondiffusive radical reactions have the single largest effect on the resulting abundances of bulk species. By comparison, cosmic-ray-driven chemistry on its own has a smaller effect at low temperatures, as the resulting thermal radiolysis products build up in the ice due to their low diffusion-based reaction rates. As we first showed in Shingledecker et al. (2019b), our Model B results further illustrate the importance of nondiffusive bulk reactions for fully and accurately simulating solid-phase radiation chemistry. Critically though, Figures 5 and 8, show that the large sulfur allotrope abundances predicted in Model B require *both* of these mechanisms.

4. Conclusions

In this work, we have examined the effects of novel modifications of astrochemical models on the abundances of sulfur-bearing species in cold cores. Specifically, we have considered the effects of, (a) a cosmic-ray-driven radiation chemistry, and (b) fast *nondiffusive* bulk reactions for radicals and reactive species.

Our main results are the following:

1. The inclusion of (a) and (b) in three-phase models results in increased bulk abundances of OCS and SO_2, leading to good agreement between the calculated and observed abundance ratios for these species in interstellar ices.
2. Moreover, (a) and (b) improved the overall agreement between the results of our simulations and the abundances of sulfur-bearing species measured by the *Rosetta* mission, shown in Table 5 (Calmonte et al. 2016).
3. Finally, the inclusion of (a) and (b) greatly increases the bulk abundance of sulfur allotropes, particularly elemental sulfur (S_8).

The nondiffusive mechanism we have used for treating the reaction of radicals in the bulk has been tested in a previous work and shown to yield far better agreement with well-constrained experiments than current approaches relying on thermal diffusion of one kind or another (Shingledecker et al. 2019b). This work is a first attempt to apply such insights to models of the ISM, and thus, Model B may represent the most realistic simulation of interstellar ice-mantle chemistry to date. Nevertheless, much work can and should still be done to improve both our chemical network as well as the physical processes simulated by the code itself.

One promising method for improving solid-phase chemical networks is to attempt to reproduce well-constrained experiments, as we have done previously with ion-irradiated pure O_2 and H_2O ices (Shingledecker et al. 2019b). In many current laboratory studies, however, the abundances of only a small number of species can be tracked during the course of the experiment using traditional techniques such as FTIR. Unfortunately, the physical properties of elemental sulfur that make it difficult to observe in the ISM make measuring its abundance in experimental ices similarly difficult. Nevertheless, S_8 can be detected using Raman spectroscopy (Anderson & Loh 1969), which may be the only practical way to estimate whether, or to what degree, such species form in sulfur-containing ice mantles under interstellar conditions.

Regarding additional physical effects resulting from bombardment by energetic particles, perhaps the most astrochemically important of these are related to the desorption of ice-mantle species. Some, such as desorption stimulated by grain heating, are currently considered in a preliminary way (Hasegawa & Herbst 1993), and could be improved with more accurate estimates related to the average amount of heating per cosmic ray as well as the rate at which such heat propagates through the ice mantle—including as a function of grain size, which Zhao et al. (2018) found could have significant effects on resulting gas-phase abundances. In addition, though, energetic particle bombardment is known to drive desorption via a number of *nonthermal* mechanisms including sputtering (Burkhardt et al. 2019) and impulsive spot heating (Ivlev et al. 2015), and attempts should be made to include such processes in future models.

C.N.S. thanks the Alexander von Humboldt Foundation for their generous support and both K. Altwegg and W.F. Thi for stimulating discussions during the course of this project. T.L. is grateful for support from the Netherlands Organisation for Scientific Research (NWO) via a VENI fellowship (722.017.008). E.H. thanks the National Science Foundation for support of his program in astrochemistry (AST 1906489). The work by A.V. is supported by the Russian Science Foundation via the Project 18-12-00351. A.V. is the head of the Partner Group of the Max Planck Institute for Extraterrestrial Physics, Garching, at the Ural Federal University, Ekaterinburg, Russia.

Software: MONACO (Vasyunin et al. 2017).

Appendix A
Chemical Network

An expanded sulfur network, a fragment of which is shown in Table 7 of this Appendix, has been used in this work. Here, R1 & 2 are the reactants, while P1–P5 represent the products. The α, β, and γ values given in Table 7 are used to compute rate coefficients, with specific formulae and reaction types given in Laas & Caselli (2019) and Semenov et al. (2010). We note that not all reaction types utilize all three parameters. For example, rate coefficients for reactions involving atomic or molecular cations and negatively charged grains are calculated using $k = \alpha\sigma_{\rm dust}\langle v_{\rm th}(i)\rangle n_{\rm dust} S_i C_{\rm ion}(\rm s^{-1})$ where α is the branching ratio given in Table 7; $\sigma_{\rm dust}$ and $n_{\rm dust}$ are the dust cross sections and volume densities, respectively; $\langle v_{\rm th}(i)\rangle$ is the thermal velocity of species i; S_i is the sticking coefficient for species i, assumed to be unity; and $C_{\rm ion}$ accounts for electrostatic effects of singly-charged ions using the formula given in Rawlings et al. (1992). Conversely, rate coefficients for reactions between neutral dust grains and electrons are given by $k = \frac{4}{3}\sigma_{\rm dust}\langle v_{\rm th}(i)\rangle n_{\rm dust}\exp\left(-\frac{T}{20}\right)(\rm s^{-1})$. In other cases all three parameters are utilized in calculating rate coefficients, e.g. in the formula $k = \alpha\left(\frac{T}{300}\right)^{\beta}\exp\left(-\frac{\gamma}{T}\right)$ ($\rm cm^3\ s^{-1}$) which is used for bimolecular gas-phase reactions and in which α is again the branching ratio, β characterizes the temperature dependence, and γ is the chemical activation energy.

Table 7
Chemical Network Used in This Work, Based on Laas & Caselli (2019)

#	R1	R2	P1	P2	P3	P4	P5	α	β	γ
1	C^+	G^-	C	G^0				1.00E+00	0.00	0.0
2	Fe^+	G^-	Fe	G^0				1.00E+00	0.00	0.0
3	G^0	e^-	G^-					1.00E+00	0.00	0.0
4	H^+	G^-	H	G^0				1.00E+00	0.00	0.0
5	H_3^+	G^-	H_2	H	G^0			1.00E+00	0.00	0.0

(This table is available in its entirety in machine-readable form.)

Appendix B
Results from Models C–E

To disentangle the effects of the various novel features we have included in our model, we have run additional simulations, detailed in Table 4. The results of these models (C–E) are shown in Figures 6–8.

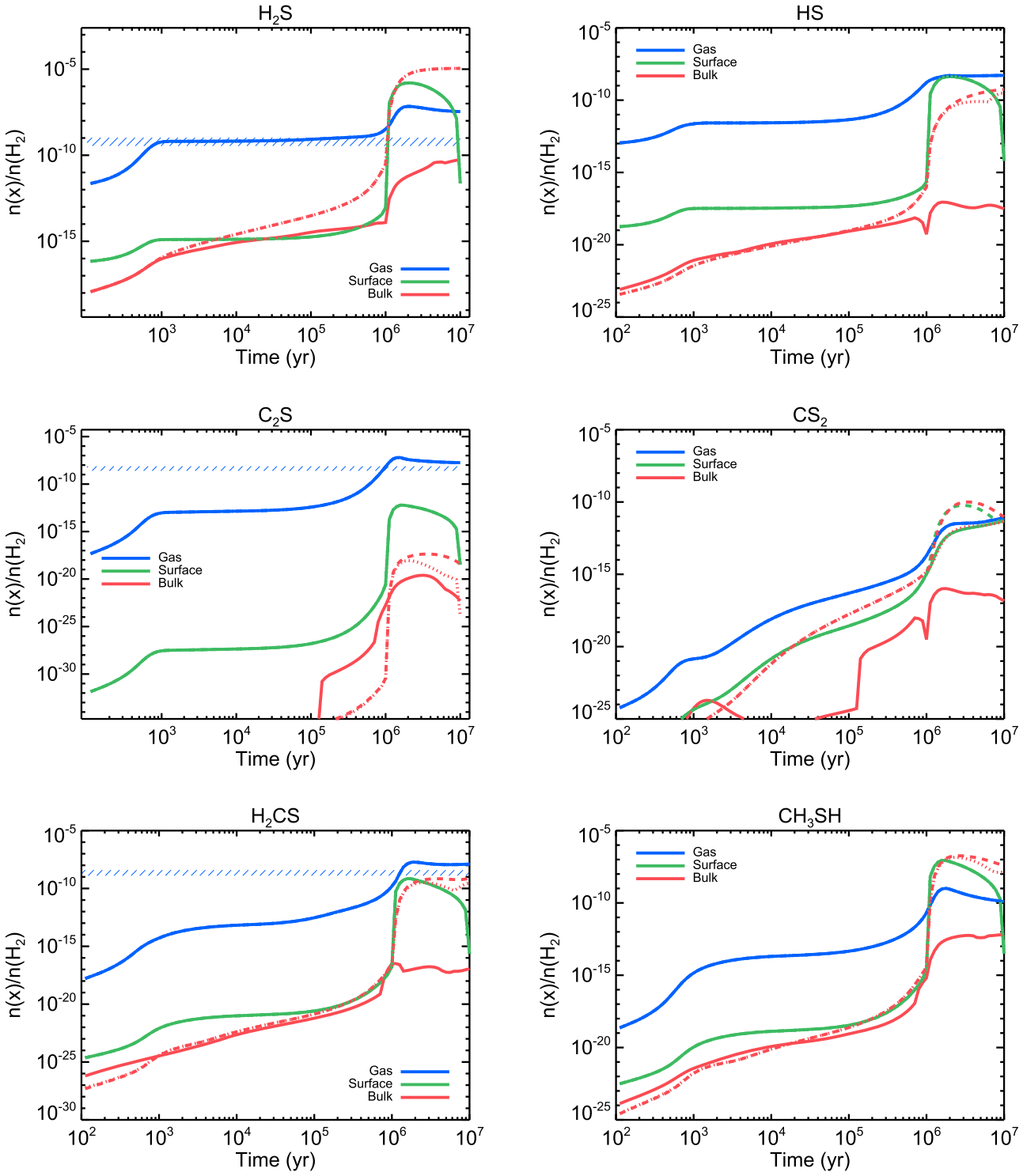

Figure 6. Calculated abundances of H_2S, HS, C_2S, CS_2, H_2CS, and CH_3SH in models C (solid line), D (dashed line), and E (dotted line). Gas-phase observational abundances for dense clouds, where available, are represented by horizontal blue hatched bars (see Laas & Caselli 2019 and references therein.).

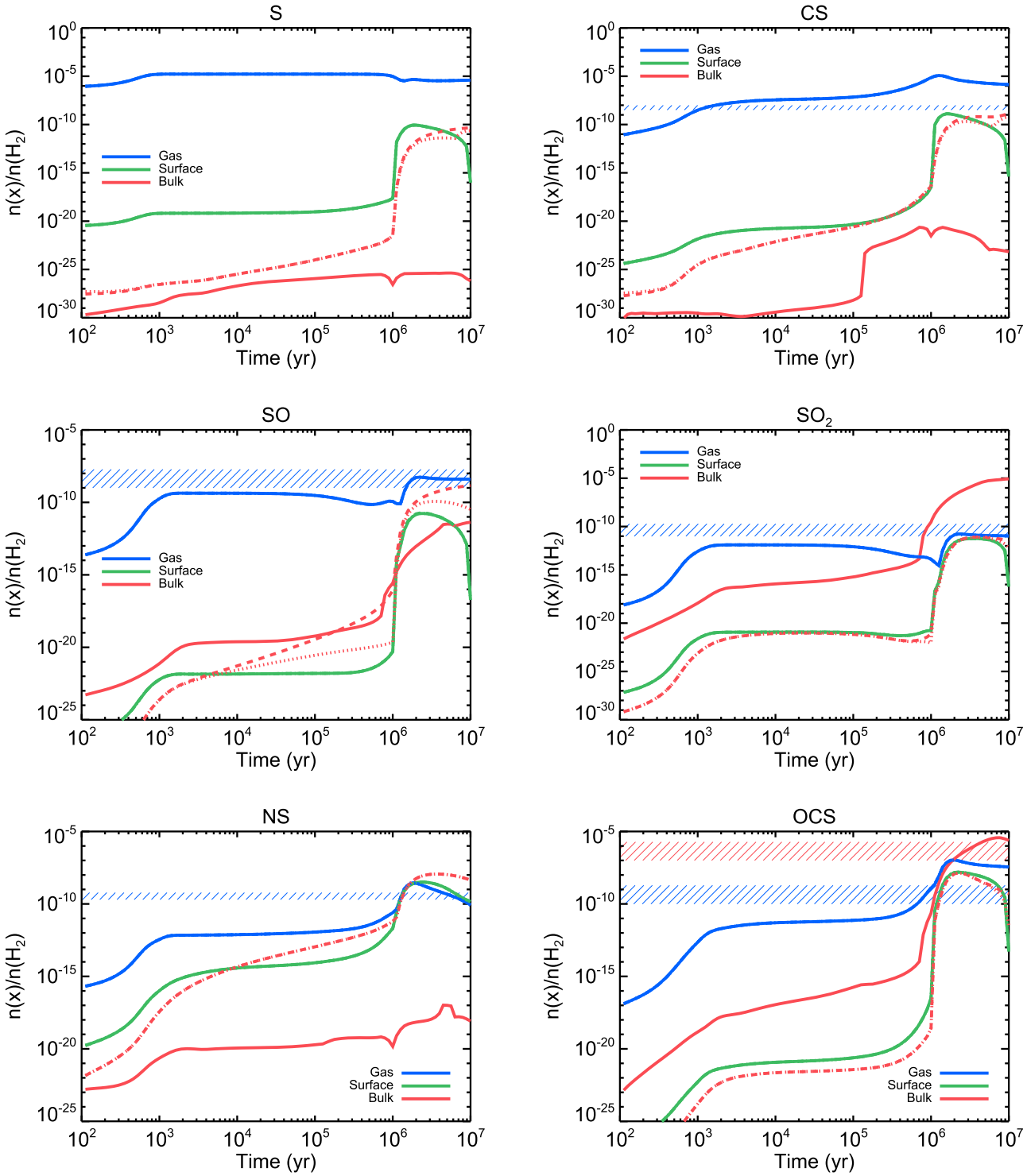

Figure 7. Calculated abundances of S, CS, SO, SO_2, NS, and OCS in models C (solid line), D (dashed line), and E (dotted line). Gas-phase observational abundances for dense clouds, where available, are represented by horizontal blue hatched bars (see Laas & Caselli 2019 and references therein.).

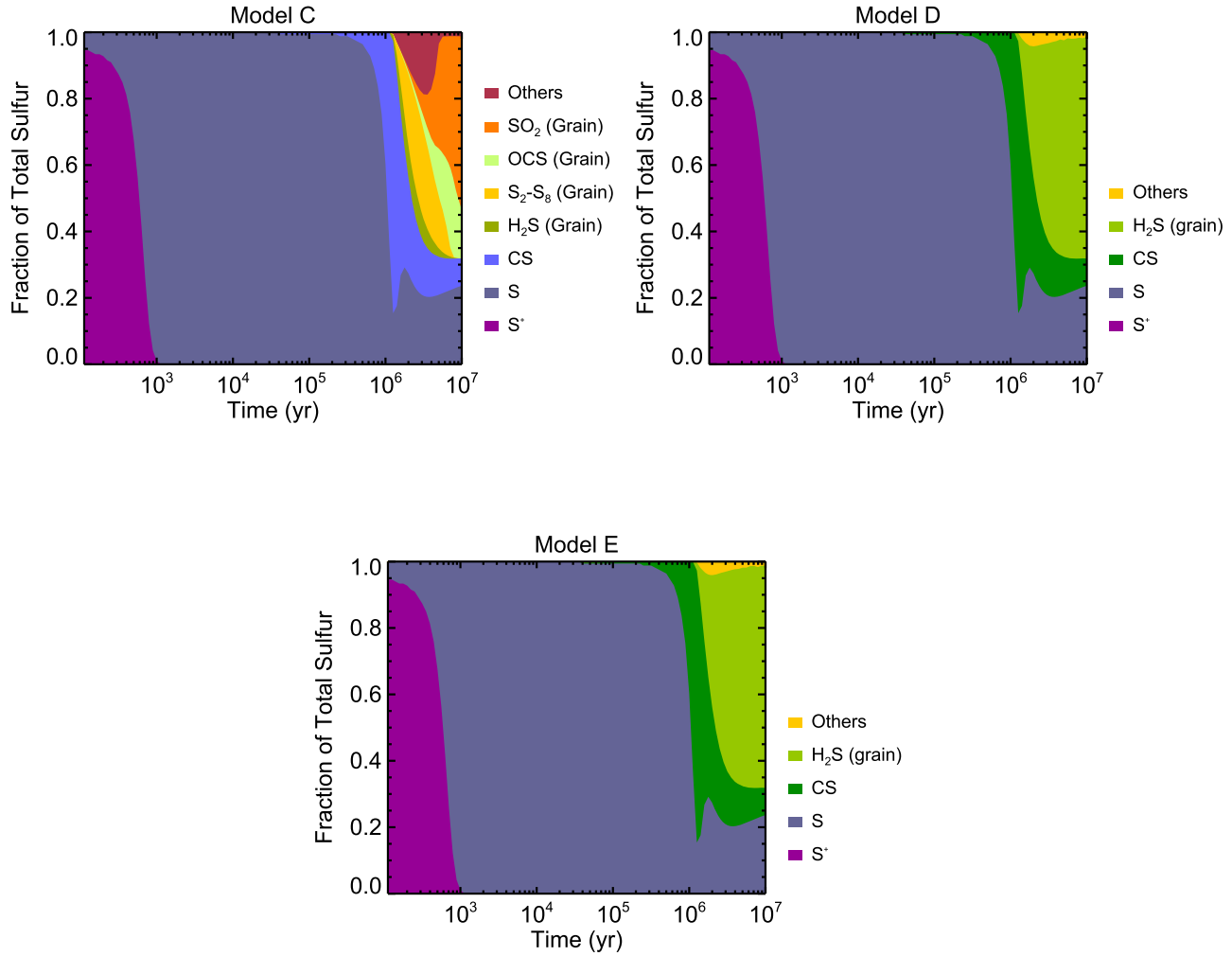

Figure 8. Main sulfur-bearing species in Models C—E.

ORCID iDs

Christopher N. Shingledecker https://orcid.org/0000-0002-5171-7568
Thanja Lamberts https://orcid.org/0000-0001-6705-2022
Jacob C. Laas https://orcid.org/0000-0001-6876-6940
Anton Vasyunin https://orcid.org/0000-0003-1684-3355
Eric Herbst https://orcid.org/0000-0002-4649-2536
Johannes Kästner https://orcid.org/0000-0001-6178-7669
Paola Caselli https://orcid.org/0000-0003-1481-7911

References

Abplanalp, M. J., Gozem, S., Krylov, A. I., et al. 2016, PNAS, 113, 7727
Agundez, M., Marcelino, N., Cernicharo, J., & Tafalla, M. 2018, A&A, 611, L1
Aikawa, Y., Kamuro, D., Sakon, I., et al. 2012, A&A, 538, A57
Anderson, A., & Loh, Y. T. 1969, CaJCh, 47, 879
Anderson, D. E., Bergin, E. A., Maret, S., & Wakelam, V. 2013, ApJ, 779, 141
Asgeirsson, V., Arnaldsson, A., & Jónsson, H. 2018, JChPh, 148, 102334
Asplund, M., Grevesse, N., Sauval, A. J., & Scott, P. 2009, ARA&A, 47, 481
Boogert, A. C. A., Gerakines, P. A., & Whittet, D. C. B. 2015, ARA&A, 53, 541
Boogert, A. C. A., Schutte, W. A., Helmich, F. P., Tielens, A. G. G. M., & Wooden, D. H. 1997, A&A, 317, 929
Burkhardt, A. M., Shingledecker, C. N., Gal, R. L., et al. 2019, ApJ, 881, 32
Calmonte, U., Altwegg, K., Balsiger, H., et al. 2016, MNRAS, 462, S253
Carlson, R. W., Kargel, J. S., Douté, S., Soderblom, L. A., & Dalton, J. B. 2007, in Io After Galileo: A New View of Jupiter's Volcanic Moon, ed. R. M. C. Lopes & J. R. Spencer (Berlin: Springer), 193
Cernicharo, J., Lefloch, B., Agúndez, M., et al. 2018, ApJL, 853, L22
Chang, Q., & Herbst, E. 2014, ApJ, 787, 135
Chen, Y.-J., Juang, K.-J., Nuevo, M., et al. 2015, ApJ, 798, 80
Cuppen, H. M., & Garrod, R. T. 2011, A&A, 529, A151
Danilovich, T., Ramstedt, S., Gobrecht, D., et al. 2018, A&A, 617, A132
Danilovich, T., Sande, M. V. d., Beck, E. D., et al. 2017, A&A, 606, A124
Drozdovskaya, M. N., van Dishoeck, E. F., Jørgensen, J. K., et al. 2018, MNRAS, 476, 4949
Dungee, R., Boogert, A., DeWitt, C. N., et al. 2018, ApJL, 868, L10
Esplugues, G. B., Viti, S., Goicoechea, J. R., & Cernicharo, J. 2014, A&A, 567, A95
Esteban, C., Peimbert, M., García-Rojas, J., et al. 2004, MNRAS, 355, 229
Fayolle, E. C., Öberg, K. I., Cuppen, H. M., Visser, R., & Linnartz, H. 2011, A&A, 529, A74
Ferrante, R. F., Moore, M. H., Spiliotis, M. M., & Hudson, R. L. 2008, ApJ, 684, 1210
Garozzo, M., Fulvio, D., Kanuchova, Z., Palumbo, M. E., & Strazzulla, G. 2010, A&A, 509, A67
Garrod, R. T. 2013, ApJ, 765, 60
Garrod, R. T., Wakelam, V., & Herbst, E. 2007, A&A, 467, 1103
Ghesquière, P., Ivlev, A., Noble, J. A., & Theulé, P. 2018, A&A, 614, A107
Gorai, P., Das, A., Das, A., et al. 2017, ApJ, 836, 70
Greenberg, J. M., & Yencha, A. J. 1973, IAU Symp. 52 Interstellar Dust and Related Topics 52 (Dordrecht: Reidel), 369
Hasegawa, T. I., & Herbst, E. 1993, MNRAS, 261, 83
Hasegawa, T. I., Herbst, E., & Leung, C. M. 1992, ApJS, 82, 167
Herbst, E., & Klemperer, W. 1973, ApJ, 185, 505

Herbst, E., & Millar, T. J. 2008, in Low Temperatures and Cold Molecules, ed. I. W. M. Smith (London: Imperial College Press)
Holdship, J., Jimenez-Serra, I., Viti, S., et al. 2019, ApJ, 878, 64
Holdship, J., Viti, S., Jimenez-Serra, I., et al. 2016, MNRAS, 463, 802
Hudson, R. L., & Gerakines, P. A. 2018, ApJ, 867, 138
Ivlev, A. V., Dogiel, V. A., Chernyshov, D. O., et al. 2018, ApJ, 855, 23
Ivlev, A. V., Röcker, T. B., Vasyunin, A., & Caselli, P. 2015, ApJ, 805, 59
Jenkins, E. B. 2009, ApJ, 700, 1299
Jiménez-Escobar, A., & Muñoz Caro, G. M. 2011, A&A, 536, A91
Kama, M., Shorttle, O., Jermyn, A. S., et al. 2019, ApJ, 885, 114
Kästner, J. 2014, Wiley Interdisciplinary Reviews: Computational Molecular Science, 4, 158
Kuwahata, K., Hama, T., Kouchi, A., & Watanabe, N. 2015, PhRvL, 115, 133201
Laas, J. C., & Caselli, P. 2019, A&A, 624, A108
Lamberts, T. 2018, A&A, 615, L2
Lamberts, T., Cuppen, H. M., Ioppolo, S., & Linnartz, H. 2013, PCCP, 15, 8287
Lamberts, T., & Kästner, J. 2017, JPCA, 121, 9736
Lamberts, T., Samanta, P. K., Köhn, A., & Kästner, J. 2016, PCCP, 18, 33021
Landau, L., & Lifshitz, E. 1976, Course of Theoretical Physics, Vol. 1, Mechanics (3rd ed.; Oxford: Butterworth-Heinemann)
Le Gal, R., Öberg, K. I., Loomis, R. A., Pegues, J., & Bergner, J. B. 2019, ApJ, 876, 72
Mihelcic, D., & Schindler, R. N. 1970, Berichte der Bunsengesellschaft für physikalische Chemie, 74, 1280
Moore, M. H., Hudson, R. L., & Carlson, R. W. 2007, Icar, 189, 409
Morgan, W. J., Huang, X., Schaefer, H. F., & Lee, T. J. 2018, MNRAS, 480, 3483
Oba, Y., Tomaru, T., Lamberts, T., Kouchi, A., & Watanabe, N. 2018, NatAs, 2, 228
Öberg, K. I., Fayolle, E. C., Cuppen, H. M., van Dishoeck, E. F., & Linnartz, H. 2009, A&A, 505, 183
Padovani, M., Galli, D., Ivlev, A. V., Caselli, P., & Ferrara, A. 2018, A&A, 619, A144
Palumbo, M. E., Geballe, T. R., & Tielens, A. G. G. M. 1997, ApJ, 479, 839
Prasad, S. S., & Huntress, W. T., Jr. 1982, ApJ, 260, 590
Prasad, S. S., & Tarafdar, S. P. 1983, ApJ, 267, 603
Przybilla, N., Nieva, M.-F., & Butler, K. 2008, ApJL, 688, L103
Rawlings, J. M. C., Hartquist, T. W., Menten, K. M., & Williams, D. A. 1992, MNRAS, 225, 471
Roessler, K. 1991, in International School of Physics "Enrico Fermi" Course CXI, ed. E. Bussoletti & G. Strazzulla (Villa Monastero: North-Holland Press), 197
Rommel, J. B., Goumans, T. P. M., & Kästner, J. 2011, Journal of Chemical Theory and Computation, 7, 690
Semenov, D., Favre, C., Fedele, D., et al. 2018, A&A, 617, A28
Semenov, D., Hersant, F., Wakelam, V., et al. 2010, A&A, 522, A42
Sendt, K., Jazbec, M., & Haynes, B. S. 2002, Proceedings of the Combustion Institute, 29, 2439
Senevirathne, B., Andersson, S., Dulieu, F., & Nyman, G. 2017, MolAs, 6, 59
Shingledecker, C. N., Álvarez Barcia, S., Korn, V. H., & Kästner, J. 2019a, ApJ, 878, 80
Shingledecker, C. N., Gal, R. L., & Herbst, E. 2017, PCCP, 19, 11043
Shingledecker, C. N., & Herbst, E. 2018, PCCP, 20, 5359
Shingledecker, C. N., Tennis, J., Gal, R. L., & Herbst, E. 2018, ApJ, 861, 20
Shingledecker, C. N., Vasyunin, A., Herbst, E., & Caselli, P. 2019b, ApJ, 876, 140
Silsbee, K., Ivlev, A. V., Padovani, M., & Caselli, P. 2018, ApJ, 863, 188
Smith, R. G. 1991, MNRAS, 249, 172
Spitzer, L., Jr., & Tomasko, M. G. 1968, ApJ, 152, 971
Steudel, R. 1982, Inorganic Ring Systems, Topics in Current Chemistry (Berlin: Springer), 149
Steudel, R., & Eckert, B. 2003, in Elemental Sulfur and Sulfur-Rich Compounds I, Topics in Current Chemistry, ed. R. Steudel (Berlin: Springer), 1
Taquet, V., Ceccarelli, C., & Kahane, C. 2012, A&A, 538, A42
Tielens, A. G. G. M., & Hagen, W. 1982, A&A, 114, 245
Vastel, C., Quénard, D., Le Gal, R., et al. 2018, MNRAS, 478, 5514
Vasyunin, A. I., Caselli, P., Dulieu, F., & Jiménez-Serra, I. 2017, ApJ, 842, 33
Vasyunin, A. I., & Herbst, E. 2013, ApJ, 762, 86
Vidal, T. H. G., Loison, J.-C., Jaziri, A. Y., et al. 2017, MNRAS, 469, 435
Vidal, T. H. G., & Wakelam, V. 2018, MNRAS, 474, 5575
Zakharenko, O., Lewen, F., Ilyushin, V. V., et al. 2019, A&A, 621, A114
Zasowski, G., Kemper, F., Watson, D. M., et al. 2009, ApJ, 694, 459
Zhao, B., Caselli, P., & Li, Z.-Y. 2018, MNRAS, 478, 2723
Zheng, J., & Truhlar, D. G. 2010, PCCP, 12, 7782